Taylor, A. C., Lautenschlager, S., Qi, Z., & Rayfield, E. J. (2017). Biomechanical Evaluation of Different Musculoskeletal Arrangements in *Psittacosaurus* and Implications for Cranial Function. *Anatomical Record: Advances in Integrative Anatomy and Evolutionary Biology*, *300*(1), 49-61. https://doi.org/10.1002/ar.23489

The Anatomical Record

Biomechanical evaluation of different musculoskeletal arrangements in *Psittacosaurus* and implications for cranial function

Journal:	*Anatomical Record*
Manuscript ID	AR-SI-ZYG-16-0079.R1
Wiley - Manuscript type:	Special Issue Article
Date Submitted by the Author:	n/a
Complete List of Authors:	Taylor, Adam; University of Bristol, Earth Sciences Lautenschlager, Stephan; University of Bristol, Earth Sciences Zhao, Qi; Institute of Vertebrate Paleontology and Paleoanthropology Rayfield, Emily; University of Bristol, Earth Sciences
Keywords:	Zygoma, Function, Evolution, dinosaur, skull

TITLE PAGE

Biomechanical evaluation of different musculoskeletal arrangements in *Psittacosaurus* - and implications for cranial function

Adam C. Taylor[1], Stephan Lautenschlager[1*], Zhao Qi[2], Emily J. Rayfield[1]

[1]School of Earth Sciences, University of Bristol, Life Sciences Building, 24 Tyndall Avenue, Bristol BS8 1TQ, United Kingdom

[2]Institute of Vertebrate Paleontology and Paleoanthropology, Chinese Academy of Sciences, PO Box 643, Beijing 100044, People's Republic of China;

*Corresponding author (email: glzsl@ bristol.ac.uk)

ABSTRACT

The masseter muscle complex is a unique feature of extant mammals and their advanced cynodont precursors, originating from the zygomatic arch and inserting on to the lateral surface of the dentary. This muscle complex is absent in sauropsids, with the exception of the neomorphic m. pseudomasseter complex that is unique to psittaciform birds (parrots and cockatiels). The anterior position and anterodorsally inclined line of action of both muscle groups increases leverage of the jaw and is thought to contribute to increased bite force, particularly in psittaciforms. A corollary is that in mammals at least, the masseter places increased load on the zygomatic arch, which may be withstood by soft tissue temporal fascia. Recently the existence of a m. pseudomasster (mPSM) and m. adductor mandibulae externus ventralis (mAMEV) has been proposed in the ornithischian dinosaur *Psittacosaurus*. Here we use computed tomography, digital restoration of skull anatomy and adductor musculature and computational biomechanics to test how the presence of anterodorsally inclined muscle loads influences stress, strain, deformation and estimated bite forces in the skull of *Psittacosaurus*. We find that the m. pseudomasseter and m. amev increases bite force with an associated increase in cranial stress and deformation. There is, however, limited osteological evidence for the existence of these two additional muscles in the psittacosaur skull and geometric morphometric informed sensitivity analysis of our finite element models shows that bite position has a greater effect on loading-induced deformation than muscle loading or material property variation.

INTRODUCTION

The integration of the zygomatic arch as a site of attachment for muscles of the jaw adductor complex is a classic hallmark of extant mammals and their cynodont precursors (Kemp, 2005). In addition, the zygomatic arch and associated structures played an important role in the differentiation of the masseter muscle (into deep and superficial components) (Abdala and Damiani, 2004) and are therefore of fundamental importance for the evolution of the mammalian feeding apparatus. The masseter muscle complex and its origin from the zygomatic arch are unique to mammals among vertebrates. The only exception are psittaciform birds (parrots), in which a neomorphic m. pseudomasseter has evolved, along with a second unique muscle, the m. ethmomandibularis (Tokita et al., 2013). Where present and well developed, the pseudomasseter covers the jugal bone laterally and inserts on the lateral surface of the mandible, bearing a superficial resemblance to the mammalian masseter. However, no other avian taxon possesses jaw muscle fibres that extend to and cover the jugal bone, and this muscle is associated with a range of parrot-specific craniofacial novelties (Tokita 2003). Similarly, no other archosaur clade (fossil and extant) has evolved a muscle complex analogous to the mammalian masseter (although an extension of the m. pterygoidues ventralis muscle that wraps around the lateral face of the mandible has been suggested for derived hadrosaurids and tyrannosaurids (Holliday, 2009)).

Nevertheless, the medially inset dentition and corresponding bony recesses on ornithischian dinosaur skulls were once assumed to be the osteological correlates of cheek muscles (Lull and Wright, 1942; Galton, 1973). While a *de novo* cheek muscle of some sort, distinct from a type of extra-oral tissue, would not be an impossible evolutionary feature, it would share no homology with the mammalian m. masseter or the m. buccinatoris since no living sauropsid features this muscle. Moreover, the medially inset dentition (suggested to be evident of a cheek on ornithischians), is generally absent in mammals (Knoll, 2008).

Recently, the presence of a muscle similar to the psittaciform m. pseudomasseter has been suggested in the ceratopsian dinosaur *Psittacosaurus gobiensis* (Sereno et al., 2010). A further expansion of the M. adductor mandibulae externus ventralis, originating from the ventral surface of the jugal horn to the lateral surface of the mandible, is also proposed. This is a novel instance of muscle reconstruction as the jaw closing musculature of dinosaurs is commonly restricted to the adductor chamber and the pterygoid region (Holliday, 2009). The muscle reconstruction supports a hypothesis of convergent cranial function and beak usage between psittacosaurs and their avian namesake, psittaciform birds, purported to increase jaw mechanical advantage as a result of supposed adaptation to eating hard foods such as nuts and seeds (Sereno et al., 2010). As birds comprise half of the extant phylogenetic bracket of dinosaurs, so at first glance, this muscle could seem more phylogenetically supported than a mammalian masseter in dinosaurs. However, the emergence of a neomorphic muscle complex in *Psittacosaurus* would represent a unique case of convergence.

In this contribution, we applied digital restoration techniques to reconstruct the cranial musculoskeletal anatomy of *Psittacosaurus lujiatunensis*, a species closely related to *P. gobiensis* (see below). Using Finite Element Analysis (FEA), an engineering technique which allows to predict the structural response of biological tissues such as bone to varied loading regimes, we simulated different hypothetical muscular configurations for *Psittacosaurus* and recorded how different muscle configurations affected cranial function, measured in terms of bony stress, strain and deformation and estimated bite forces. The proposed existence of a m. pseudomasseter and m. adductor mandibulae externus ventralis in psittacosaurs allowed us to test how muscular loading of the jugal bar modifies skull mechanical behaviour.

Anatomical abbreviations— bc, braincase; **ex**, exoccipital; **f**, frontal; **j**, jugal; **l**, lacrimal; **mAME**, m. adductor mandibulae externus; **mAMEM**, m. adductor mandibulae externus medialis; **mAMEP**, m. adductor mandibulae externus profundus; **mAMES**, m. adductor

mandibulae externus superficialis; **mAMEV**, m. adductor mandibulae externus ventralis; **mAMP**, m. adductor mandibulae posterior; **mAMI**, m. adductor mandibulae internus; **man**, mandible; **mDM**, m. depressor mandibulae; **mPSTp**, m. pseudotemporalis profundus; **mPSTs**, m. pseudotemporalis superficialis; **mPSM**, m. pseudomasseter; **mPTd**, m. pterygoideus dorsalis; **mPTv, m**. pterygoideus ventralis; **max**, maxilla; **n**, nasal; **p**, parietal; **pf**, prefrontal; **pmx**, premaxilla; **po**, postorbital; **pt**, pterygoid; **q**, quadrate; **qj**, quadratojugal; **r**, rostral; **sq**, squamosal

MATERIAL AND METHODS

Specimens and digitisation

For this study, the skull of *Psittacosaurus lujiatunensis* (IVPP V12617, Institute of Vertebrate Paleontology and Paleoanthropology) (Fig. 1A) was CT scanned at IVPP in Beijing, where the specimen is housed. This specimen was first described as an adult paratype of *Hongshanosaurus houi* (You and Xu, 2005). *Hongshanosaurus* is a second nominal genus within the Psittacosauridae, the holotype of which is a juvenile skull, distinguished from *Psittacosaurus* by having an elliptical orbit and lower temporal fenestra with the major axis oriented caudodorsally (You et al., 2003). However, 3D geometric morphometrics reveal that *H. houi*, as well as *Psittacosaurus lujiatunensis* and *P. major*, are in fact synonymous, representing different taphomorphotypes of *P. lujiatunensis* (Hedrick and Dodson, 2013). This means that the observed geometric variation between specimens is caused by taphonomic distortion and does not qualify as interspecific variation. Thus, the specimen studied in this paper (IVPP V12617) was renamed as *P. lujiatunensis* (Hedrick and Dodson, 2013).

Digital restoration and reconstruction

The final CT data set, consisting of 1200 image slices (1126 x 1296 x 1200 pixels, 141 µm voxel size) were imported into AVIZO (version 8.1.1, Visualization Sciences Group) where individual skull elements were separately labelled using the AVIZO segmentation editor. Due to some taphonomic distortion and preservational artefacts (Fig. 1B), the osteology of the specimen had to be restored digitally (Lautenschlager et al., 2014) before a muscle reconstruction was performed. Of the paired bones of the skull, only the elements on the right side of the cranium were labelled, except the nasals and prefrontals, for which both left and right elements were labelled considering ~~due to~~ their medial position along the central axis of the skull. Paired elements were then mirrored in groups to produce an osteological reconstruction of the external bones of the cranium. The bones around the braincase as well as the palatine and vomers were not included in this initial reconstruction ~~due to~~because of the fused nature of th~~e~~is ~~akinetic~~ skull (You and Xu, 2005) which meant identification of separate bones was not always possible in the central region of the cranium. The rostral and parietal bones were mirrored to fill in cracks and missing segments in these bones. All other elements of the skull and the lower jaw were repaired by automatically interpolating between complete sections, or by manually using the paintbrush tool in the AVIZO segmentation editor, depending on the size and geometric complexity of the break. To remove taphonomic distortion, the right side of the cranium was mirrored to fit the left, producing a more symmetrical model. No biological system is ever perfectly symmetrical, but to remove the possibility of artefact creation in the finite element model, a mirrored reconstruction was created (Fig. 2). Teeth were labelled separately to bone, and missing teeth were filled in by duplicating then fitting complete teeth into the gaps where tooth sockets were visible.

Muscle attachment sites were identified following a method of osteological and homological deduction (Bryant and Russell, 1992; Holliday, 2009; Lautenschlager, 2013). Firstly, depressions or ridges indicative of muscle attachment sites were identified, paying attention to the topology implied by adjacent muscle attachments (Lautenschlager, 2013). Secondly, study of muscle attachments in extant archosaurs allowed for identification of homologous muscles, which have previously been identified in the adductor chambers of many non-avian dinosaurs (Holliday, 2009). Finally, two additional muscle attachments were labelled, m. adductor mandibulae externus ventralis (mAMEV) and m. pseudomasseter (mPSM), following a previous reconstruction (Sereno et al., 2010), tested in the present study.

The attachment and origin sites were labelled in the dorsoventral plane using the selection tool in AVIZO and the selected areas were interpolated between to produce a straight-lined approximation of muscle position. These were adjusted in shape to prevent cross-cutting of bone or other muscle surfaces, and then iteratively increased in size to fill the whole adductor chamber (Fig. 3).

Muscle and bite forces

Muscle volumes (Table 1) were measured using the AVIZO material statistics module and three dimensional lengths for each muscle were measured using the AVIZO measurement tool. Cross-sectional areas were then calculated for each muscle using equation 1, and estimates of muscle force (Table 1) were calculated by multiplying cross-sectional area by an isometric stress value ($\sigma = 0.3$ N/mm^2) (Thomason, 1991) (equation 2). It was assumed that all muscles were parallel fibered rather than pennate.

$$CSA = volume / length \quad (1)$$

$$F_{mus} = CSA \times \sigma \quad (2)$$

Next, the angle created by the main line of action exerted by the adductor muscles was measured in the sagittal plane and the resultant muscle force calculated (equation 3). Finally, the outlever length (distance between jaw joint and bite point) and the inlever length (perpendicular distance from the line of action to the jaw joint) were measured in IMAGEJ (Abramoff et al., 2004) to produce bite force estimations (equation 4) (Lautenschlager, 2013). Three different bite force estimates were calculated, corresponding to bite positions at the beak, the anterior-most tooth, and the posterior-most tooth.

$$F_{res} = F_{mus} \times \cos\alpha \quad (3)$$

$$F_{bite} \times L_{outlever} = F_{res} \times L_{inlever} \quad (4)$$

Following finite element analysis (see following paragraph), reaction forces were measured at the bite point constraints on both the cranium and the mandible. This method calculated maximum bite forces during feeding as the finite element model considers the topology of the whole skull and all muscles. A range of values was generated ~~due to~~ to account for differences in the value recorded on the cranium and the mandible.

Finite element analysis

Surface models for the cranium and mandible were exported from AVIZO into HYPERMESH (versions 11.0 and 13.0, Altair Engineering) to create a solid mesh of tetrahedral ~~nodes~~elements. 490,143 ~~nodes~~ elements were generated for the cranium model and 446,865 ~~nodes~~ elements were generated for the mandible model. Material properties of bone and enamel were applied in HYPERMESH, based upon phylogenetically appropriate modern analogues since no exact property values are known for dinosaur bone or enamel. The material properties of alligator mandibles (E = 20.49 GPa, υ = 0.40 [Zapata et al., 2010]) and crocodile teeth (E = 60.40 GPa, υ = 0.31 [Creech, 2004]) were used, following the

methodology of a study of the therizinosaurid dinosaur, *Erlikosaurus andrewsi* (Lautenschlager et al., 2013).

Constraints were applied in HYPERMESH to replicate the attachment of the skull to the rest of the body at the neck. Nodes around the occipital condyle and the sites of attachment of craniocervical muscles on the exoccipital and squamosal were constrained from motion in all directions. Constraints were also applied at the surface of articulation on the quadrate and articular to replicate the articulation of the jaw joint on both the cranium and the mandible. A final set of constraints were applied to simulate three different bite points: (i) at the beak, (ii) bilateral biting at the anterior-most tooth, and (iii) bilateral biting at the posterior-most tooth.

Muscle loads were applied in HYPERMESH to the relevant attachment sites. The muscle force for each muscle was divided by the number of nodes used to load the model for each attachment site. Larger attachment sites required the muscle force to be distributed over a greater number of nodes, so that the whole attachment surface was loaded rather than just individual points experiencing the whole muscle force. The HYPERMESH models were saved as multiple input files (.inp) to test the three different bite points. Different arrangements of muscles were saved separately to ascertain the function of the mAMEV and mPSM during simulated feeding. Four muscle combinations were tested for each bite point: (i) the standard jaw adductor muscles with strong phylogenetic support that are homologous to all archosaurs (mStd), (ii) mStd plus mPSM, (iii) mStd plus mAMEV, and (iv) mStd plus both mPSM and mAMEV. 24 input files were saved, 12 for the cranium and 12 for the mandible.

A further 32 FE analyses were then undertaken to ascertain the effect of material properties upon the anterior-most tooth and posterior-most tooth bite models. The beak bite models were not tested under sensitivity analyses as none of the nodes actively constrained or loaded for this bite point had the material properties of teeth. For the beak bite models, the bite point was constrained on the rostral and the predentary bones. Therefore, to make the

most of the sensitivity analyses and test the effect of altering the material properties of teeth as well as bone, only the anterior-most tooth and posterior-most tooth bite models underwent sensitivity tests. The elastic modulus for both teeth and bone were respectively increased or decreased by 10% in HYPERMESH, giving a further two input files saved for each of the original (material properties ±10) finite element models.

All 56 input files were exported from HYPERMESH into ABAQUS (versions 6.10 and 6.14, Simulia) to solve the finite element models. The results files were visualised as Von Mises stress plots with a blue-red scale where lowest stresses are blue and higher stresses are red. The scale was changed from a discrete to a continuous scale, with minimum limits set to 0 MPa and maximum scale limits set as 3 MPa for the cranium and 10 MPa for the mandible.

Geometric morphometric analysis

We used a geometric morphometric (GMM) approach to quantitatively compare variation in how the skull deforms when different loading conditions (muscle groups and bite points) are applied. This approach is described in detail by O'Higgins et al. (2011) and has been employed in recent papers (~~REFs~~Cox et al., 2011; Parr et al., 2012; Lautenschlager et al., 2016). When the skull experiences an applied load it may deform the finite element mesh. By recording the three-dimensional coordinates of certain nodes comprising the apices of the elements, the relative positions of these nodes can be compared between different models to define how different loading conditions variably deform the skull. The three dimensional coordinates of 68 homologous landmark points~~s~~ were acquired for the undeformed model and each of the deformed models using the node query tool in ABAQUS. 42 of the landmarks covered the geometry of the cranium and 26 covered the geometry of the mandible. A number of nodes that represent anatomical landmarks were selected based upon those used in a study of taphonomic variation amongst psittacosaurids (Hedrick and Dodson, 2013). This

study analysed multiple different specimens and therefore used strictly anatomical landmarks which could be identified in all specimens. However, this current study features a single specimen with the same mesh used for each finite element model. This meant that any landmark node chosen would be homologous between the undeformed model and each of the deformed models. On the cranium, 24 anatomical landmarks from the previously mentioned study (Hedrick and Dodson, 2013) were used, and a further 18 landmarks were ~~used~~ selected to cover the whole geometry of the skull. Hedrick & Dodson (2013) focused solely on the cranium, hence ~~the~~ 26 mandibular landmarks were chosen by us to represent full coverage of mandibular morphology. The landmarks were selected from areas which avoided the points of constraint or loading where possible, as these could heavily influence the result of the analysis. Non anatomical landmarks were distributed widely across the skull to capture the full geometry and extent of deformation. The 3D nodal coordinates were entered into PAST (Hammer et al., 2001) for Procrustes analysis and principal component analysis.

RESULTS

Musculature descriptions

m. adductor mandibulae externus (mAME) group (Fig. 3)

The mAME group includes three muscles, the m. adductor mandibulae externus superficialis (mAMES), the m. adductor mandibulae externus medialis (mAMEM), and the m. adductor mandibulae externus profundus (mAMEP) (Holliday and Witmer, 2007). We find that the mAMES originates on the lateral and medial side of the temporal bar, and attaches to the dorsolateral surface of the surangular (Fig. 3A, B, E, F) (Haas, 1955; Ostrom, 1964). The mAMEM originates from the caudolateral border of the supratemporal fenestra on the squamosal, and inserts on the caudal most aspect of the coronoid process (Fig. 3A, B, C).

The mAMEP originates from the caudomedial border of the supratemporal fenestra on the parietal ridge and inserts on the coronoid process (Holliday 2009) (Fig. 3E. F).

m. adductor mandibulae internus (mAMI) group

The mAMI group includes the m. pseudotemporalis superficialis (mPSTs), the m. pterygoideus dorsalis (mPTd), and the pterygoideus ventralis (mPTv) muscles. The mPSTs originates from the rostromedial border of the supratemporal fenestra and inserts upon the rostral medial surface the mandibular fossa (Fig. 3C, D) (Ostrom, 1966). The mPTd originates from the rostral surface of the pterygoid process and attaches to the medial side of the articular (Fig. 3D, E) (Witmer, 1997). The mPTv originates from the caudal surface of the pterygoid process, and inserts upon the lateral side of the articular and surangular (Holliday 2009) (Fig. 3A, B, D, E).

m. adductor mandibulae posterior (mAMP) group

This muscle group contains just one muscle, of the same name, which originates on the lateral surface of the quadrate and attaches to a clear depression on the medial side of the mandible (Holliday 2009) (Fig. 3A, D, E, F).

m. pseudomasseter (mPSM) and m. adductor mandibulae externus ventralis (mAMEV)

Osteological correlates for the m. pseudomasseter (mPSM) and m. adductor mandibulae externus ventralis (mAMEV) are much more poorly defined, and have been placed following the reconstruction of Sereno et al., (2010). According to Sereno et al. (2010), the mPSM originates from a ridge between the premaxilla and maxilla, and inserts on the dorsal surface of the dentary in a position just rostral to the coronoid process (Fig. 3A, B,

C, F). The mAMEV originates from the ventral margin of the jugal and attaches to the lateral surface of the dentary, extending to its ventral margin (Fig. 3A, B, C)

Muscle and bite forces

Muscle volumes and forces were calculated for each muscle (see Table 1). The initial bite force estimates calculated suggested that *P. lujiatunensis* would have had a maximum estimated bite force of 46.2 N at the beak and 90.6 N at the posterior-most tooth. These values are based upon calculations of inlever and outlever ratios, and do not include the more anteriorly positioned mPSM or mAMEV. The mAMES, being the largest muscle, is capable of producing the largest force of 88.8 N, contributing 20% of the total muscle force when all muscles (including mPSM and mAMEV) are active. At the other end of the spectrum, the mPTd muscle produces the smallest force upon contraction of 11.6 N, contributing just 3% to the total muscle force. The force produced by the mPSM upon contraction is 29.9 N, or 7% of total muscle force, and the mAMEV is capable of producing 42.6 N of force (10% of total muscle force). Together, these two ambiguous muscles account for a relatively small proportion of muscle force. However, due to their anterior position, the effect on the lever mechanics of the jaw will be relatively great.

Of the three major muscle groups, the mAMI group (mPTd, mPTv, and mPSTs) has the smallest contribution to total muscle force at just 15%. The mAME group (mAMES, mAMEM and mAMEP) has the largest contribution to total muscle force, making up 44% of total muscle force when all muscles are active.

The reaction forces measured from the solved finite element model for the standard musculature (all muscles except mPSM and mAMEV) are smaller than those estimated with the dry skull method. It is shown that maximum bite force at the beak would be between 11.8 N and 30.7 N, and between 23.2 N and 74.4 N at the posterior-most tooth (Fig. 4). A range of

bite forces is generated ~~due to variation in the~~because the estimated reaction force ~~measured~~ differs between~~on~~ the cranium and on the mandible. Because 12 different finite element models were solved (three different bite points and 4 different muscle combinations) it is possible to ascertain the effect of each of the hypothesised muscles on bite force. When measured on the cranium, the bite force at the beak more than doubles from 11.8 N to 23.7 N with the inclusion of mPSM and mAMEV. The effect of these muscles is considerably less drastic when measured on the mandible, with an increase of 12.9 N (from 30.7 N to 43.6 N). At the posterior-most tooth, the maximum bite force increases by 24.3 N (from 74.4 N to 98.7 N) with the inclusion of mPSM and mAMEV.

For the beak bite and the anterior tooth bite, mAMEV causes a greater increase in bite force than the mPSM. At the beak, bite force increases by 7.5 N with mAMEV compared to 5.3 N with mPSM, and at the anterior-most tooth, bite force increases by 11.2 N with mAMEV compared to 9.1 N with mPSM. However for the posterior tooth bite, the opposite pattern is displayed. Bite force increases by 3.7 N with m AMEV compared to 8.5 N mPSM. Thus, suggesting that mPSM has a greater effect on the posterior end of the tooth row, whereas mAMEV has a greater effect at the anterior end of the skull.

Finite element analysis

12 different finite element models were solved to test different myological combinations and to simulate three different bite positions. Figure 5 shows the Von Mises stress plots for the various tested scenarios. To assist in the visualisation of these plots, separate scales are applied for the cranium and for the mandible (maximum limit of 3 MPa and 10 MPa respectively).

mStd musculature models

The FEA results for the phylogenetically supported musculature (mStd) reveal that the distribution of Von Mises stress, particularly in the mandible, is dependent upon the bite point constrained (Fig. 5A, E, I). In general, the highest cranial stresses are recorded around the supratemporal fenestra within the postorbital, squamosal and parietal; this is to be expected due to the majority of muscles attaching on or around these bones. The highest mandibular stresses are recorded anteriorly on the surangular and on the dorsal surface of the dentary.

The posterior-most tooth bite appears to show the lowest average distribution of stress across the skull, with large areas of minimal (less than 0.25 MPa) stress across the nasals, premaxillae, and rostrum. The posterior-most tooth bite shows a higher distribution of stress at the ventral margin of the lateral temporal fenestra than the other two bite points. The beak bite point seems to show a higher average stress distributed across the whole skull including higher stresses on the ventral surface of the lower jaw as well as higher stresses across the nasals and prefrontals and at the ventral and anterior margins of the orbit.

mStd+mPSM musculature models

The finite element models which included the hypothesised pseudomasseter muscle showed greater stress distributed across the skull (Fig. 5B, F, J). Again, the posterior-most tooth bite appears to have the lowest average distribution of stress across the skull while the beak bite appears to have the greatest average stress. For the beak bite, the stresses that were previously evident across the nasals and prefrontals (under the mStd musculature loading) now extend anteroventrally down the nasals towards the rostral element at the tip of the beak. Similarly, the anterior-most tooth bite model shows a small increase in stress in this area of the cranium. The posterior-most tooth bite model shows an area of stress extending laterally

across the jugal, which is similarly observed in the anterior-most tooth bite model, but to a smaller extent.

mStd+mAMEV musculature models

The inclusion of the hypothesised mAMEV muscle causes an increase in the stress induced in the skull compared to the mStd musculature model (Fig. 5C, G, K). The addition of this muscle causes a consistent increase in the stress observed on the jugal and around the ventral margin of the orbit. Similarly to the pseudomasseter, this muscle causes an increase in the stress observed on the skull roof and on the nasals for the anterior-most tooth bite and the beak bite, but for not the posterior-most tooth bite.

mStd+mPSM+mAMEV musculature models

Individually the two hypothetical muscles (mPSM and mAMEV) both clearly increase the stresses induced in the skull; when both active together with the standard jaw adductor musculature, the effects appear to be further exaggerated (Fig. 5D, H, L). The beak bite model features higher average stress, with large areas of stress around the supratemporal fenestra, at the anteroventral margins of the orbit, and down the nasals, premaxillae and rostral. For the beak bite model, high stresses are distributed more evenly across the mandible, but are especially evident on the surangular. For the posterior-most tooth bite model, stresses appear to be concentrated in the central areas of the cranium, on the basisphenoid and pterygoids, and more medially on the mandible compared to the other two bite points.

Geometric morphometric analysis

The combined FEA/GMM method (O'Higgins et al., 2011) is novel and less common in palaeontological analyses than the individual use of GMM or FEA. Other assessments of FEA results are well established, however, these have often focused on comparing strains at individual points (Metzger et al., 2005), rather than examining larger scale deformations of the whole model (O'Higgins et al., 2011). Few studies have used GMM to directly analyse FEA results (see Cox et al., 2011; O'Higgins and Milne, 2013; Polly et al., 2016).

Figure 6A shows the first two components from the GMM analysis of the 42 cranial landmarks for all 20 of the cranial finite element models. It is clear that bite point has a significant effect upon the finite element results. Principal component 1 accounts for 54.1% of variation and effectively distinguishes between different bite scenarios. Principal component 2 accounts for 22.0% of variation and distinguishes between whether or not the mAMEV muscle is active in the analysis. For all bite points, the mStd+mPSM+mAMEV and mStd+mAMEV models plot more closely to each other than to the mStd or mStd+mPSM models. It is noteworthy, that altering the material properties ± 10% has a smaller effect on cranial deformation than altering the muscle combinations.

Figure 6B shows the first two components from the GMM analysis of the 26 mandibular landmarks for all 20 of the various finite element models. Principal component 1 accounts for 92.0% of variation and, as with figure 6A, distinguishes between different bite scenarios. Principal component 2 accounts for only 4.6% of variation and distinguishes different muscle loads and variation in material properties. This shows that for the mandible, bite position accounts for most of the variation in deformation between finite element models, much more so than the variation in deformation generated by varying muscle input and material properties.

DISCUSSION

Musculoskeletal reconstruction and hypotheses

Apart from the mPSM and the mAMEV, all of the muscles reconstructed for *Psittacosaurus lujiatunensis* have strong phylogenetic support (Holliday, 2009) and are deeply homologous within archosaurs. These seven muscles (referred to as 'mStd,' here) all recently been reconstructed in various dinosaurs, including theropods (Lautenschlager, 2013; Cuff and Rayfield, 2015), sauropods (Button et al., 2014), and ornithischians (Norman et al., 2011) on the basis of osteological correlates found through the vast majority of Dinosauria (Holliday, 2009). In contrast, the osteological evidence for a pseudomasseter-like muscle in psittacosaurs is based upon analogies between the two organisms, such as strengthening of the bill margins and a sliding jaw articulation (Sereno et al., 2010). However, there are derived osteological features observed in parrots that are absent in psittacosaurs and *vice versa*. For example, parrots have a pseudoprokinetic, craniofacial hinge, (unlike the standard prokinetic, nasal-frontal hinge seen in some other birds). This is brought about by transformation of dermal bones and is considered an essential adaptation to eating hard foods (Tokita, 2003). Psittacosaur skulls are ~~strictly~~ akinetic, because despite bearing patent otic and palatobasal joints, many cranial sutures are coosified and there is no obvious potential for bone and joint movement ~~featuring coosification of many cranial sutures~~ (You and Xu, 2005; Sereno et al., 2010).

Furthermore, the mPSM in parrots attaches to another novel osteological feature that is absent in psittacosaurs, the suborbital arch, the evolution of which is shown to be just as complex as the processes leading to the unique musculature of parrots. ~~Due to t~~The ~~anatomical association of the~~ suborbital arch and mPSM ~~it was~~were once assumed ~~that~~ to be ~~they were~~ part of the same evolutionary complex (Zusi, 1993), however, it is now known that these two characters evolved independently of each other (Tokita et al., 2007). When mapped onto the psittaciform phylogeny it is shown that some parrot species acquired a suborbital

arch without the accompanying development of a pseudomasseter and *vice versa* (Tokita et al., 2007). This means the two features evolved as a result of heterochrony and/or modularity in development (Tokita *et al*., 2007). Recently, further character mapping and ancestral state reconstruction of the suborbital arch has shown that it has evolved repeatedly, with is absence representing the ancestral state (Carril *et al*., 2015). Conversely, ancestral state reconstruction of the m. pseudomasseter and the m. ethmomandibularis shows a single evolutionary origin and their absence (which is the derived condition) has evolved multiple times only within the psittaciform lineage (Carril et al., 2015), representing a deep homology and a common developmental process (Tokita *et al*., 2013).

The proposed novel muscles, mPSM and mAMEV are reconstructed on a hypothetical basis, as they have no phylogenetic support and limited osteological support within psittacosaurs. The parrot m. pseudomasseter and ethmomandibularis are associated with an alteration in *Hox* gene regulation, which causes spatially unique populations of muscle connective tissues to be derived from the cranial neural crest cells (Tokita *et al.,* 2013). This special developmental modification is acquired only in the common ancestor of all parrot species (Tokita et al., 2007), thus making the making the m. pseudomasseter unique to Psittaciformes.

The second novel muscle reconstructed in psittacosaurs, the mAMEV is only differentiated from the adductor mandibulae musculature among archosaurs in Psittaciformes (Sereno, 2012), which as mentioned, feature evolutionary and developmentally complex alterations to the jaw adductor musculature and craniofacial skeleton. Moreover, the name mAMEV is only used infrequently in studies of psittaciform musculature, as it is in fact synonymous with the more accepted mAMES (Carril *et al.,* 2015; but see Holliday & Witmer [2007] where the mAMEV is synonymized with the mAMEP). In parrots, this muscle constitutes part of the externus muscle group. In *Psittacosaurus gobiensis*, the mAMEV and

the mAMES have previously been reconstructed separately, and in addition to each other, despite their synonymy in parrots. The mAMES has been reconstructed as part of the mAME muscle group, while mAMEV is shown as a separate muscle mass, originating on the ventral side of the skull (Sereno et al., 2010). Thus, the reconstruction of *Psittacosaurus gobiensis* (featuring both the mAMEV and the mAMES) is unfounded. The only other non-psittaciform study to use the muscle name mAMEV was in a reconstruction of the jaw adductor musculature of *Heterodontosaurus* (Sereno, 2012). By the authors own admission, the reconstruction of this muscle in *Heterodontosaurus* is speculative.

The musculature reconstruction of *P. gobiensis*, tested within this study, is only presented as a single two-dimensional figure in the original publication (Sereno et al., 2010); however, when the muscles are digitally reconstructed and visualised here in three-dimensions (see Fig. 3), the constraints of the skull upon muscle topology are more apparent. The angle to which the jaw can open is limited by the length of the jaw adductor muscles (Tanoue et al., 2009; Lautenschlager, 2015), and due to their anterior position, the mPSM and the mAMEV muscles would have had a significant effect upon the maximum gape that could have be produced. At wide gapes, these muscles would be stretched far beyond their resting lengths, and consequently the maximum active tension that can be produced will be significantly diminished (Gordon et al., 1966a, 1966b; Lautenschlager, 2015).

Analysis of FEA/GMM results

The FEA/GMM results show several key points: (i) the mandible is more affected by variation in loading conditions than the cranium, (ii) bite position has a greater effect on deformation patterns than muscle loadings or material properties, (iii) the anterior-most tooth bite is more affected by changes in material properties compared to the posterior-most tooth

bite, and (iv) the posterior-most tooth bite is more greatly affected by changes in muscle loadings compared to the anterior-most tooth bite.

This first point, the fact that the mandible shows greater variation than the cranium, is expected since the mandible transmits a greater bulk of muscle forces compared to the cranium (Lautenschlager et al., 2013). The second point is ~~corroborated~~ at odds with~~by~~ the conclusions of a previous, methodologically similar study on rodents (Cox et al., 2011), which found that bone stiffness had the strongest influence on the FEA results, followed by bite position, and then bite angle. One possible reason for bone stiffness having the greatest effect on the results in the aforementioned study is because the amount of variation of material properties was much greater than in the present study. Here we increased and decreased material properties by a factor of 10%, whereas Cox et al (2011) increased and decreased material properties by a factor of around 50% ~~(Cox et al., 2011)~~. Aside from material properties, the next most determinate factor upon the FEA results was shown to be bite position (Cox et al., 2011), as was also evident in the results of this study. Our results concur with Walmsley et al. (2013) who found that bite position influenced FE-results more than the incorporation of isotropic heterogeneous and homogenous properties, and Fitton et al. (2012) ~~-~~ who found that bite position generated greater variation in strain outputs than muscle force activation in the crania of macaques.

The pattern of results for the anterior-most tooth bite point seem to match the findings of Cox et al. (2011) with material properties having a greater effect than muscle loadings: the variation in the FEA results is more dependent upon alteration of the material properties than presence or absence of the ambiguous mPSM and mAMEV muscles. On the other hand, results of the posterior-most tooth bite point demonstrate that the pattern of musculature loading and the presence or absence of the mPSM or mAMEV causes a significant change to the pattern of deformation in the skull. For this bite point, the inclusion of mPSM or mAMEV

causes changes in deformation that are beyond the range that could be induced by altering the material properties by 10%.

Bite forces and dietary implications

The bite force results (see Fig. 4) show the clear effect of the anteriorly positioned muscles (mPSM and mAMEV) upon the lever mechanics of the jaw. The effect of the bite point at the posterior-most tooth and at the beak are considered most indicative of the feeding ability of psittacosaurs, as the beak is the triturating surface that would be used to crack nuts (under the hypothesis of Sereno et al. [2010]) and the posterior most tooth experiences the greatest bite force which would act as the limiting factor on the dietary material that could be consumed.

In a study of the Monk Parakeet, *Myiopsitta monachus*, empirical bite force was calculated as 16.7 N (Carril et al., 2015). This is lower than that measured for *Psittacosaurus lujiatunensis*, but still in the broad range of bite forces, which ranged from 11.8 N to 30.7 N at the beak with the mStd musculature. The maximum bite force at the beak increased to 43.6 N with the inclusion of the mPSM and mAMEV. The bite force of *Psittacosaurus lujiatunesis* increased significantly at the caudal end of the tooth row~~, due to a~~ as the output lever length reduces and the ~~reduction of the output lever length and the~~ bite point ~~being~~ is nearer the zone of maximum input force (Tanoue *et al.* 2009). The bite force at the posterior-most tooth is between 23.2 N and 74.4 N with the mStd musculature, which increases to between 42.1 N and 98.7 N with the inclusion of the mPSM and mAMEV.

While the bite force of *Psittacosaurus lujiatunensis* is greater than that of *M. monachus*, it should be noted that the difference in body size between psittacosaurs and parrots is great. Psittaciform birds have a bite force to body mass ratio much greater than many other birds, including raptors which have morphologically similar beaks to parrots

(Carril *et al.* 2015). The maximum muscle force exerted by *Myiopsitta monachus* was calculated at 33.9 N, resulting in a maximum bite force of 16.7 N. This means that approximately 50% of the available muscle force can be transferred into bite force in *Myiopsitta monachus*. In comparison, of the maximum muscle force of 432.2 N produced by the m. Std muscle arrangement in *Psittacosaurus lujiatunensis*, less than 20% (74.4 N) is transferred to bite force. The jaw of psittaciform birds is a much more efficient lever than the psittacosaur jaw.

Moreover, the beak shape of parrots is considerably more sharp and pointed than that of psittacosaurs, meaning that the force that could be applied at the beak is concentrated over a smaller area than the rounded, flat beak of psittacosaurs. The beak shape of parrots is in fact more similar to neoceratopsians than to psittacosaurs. It has been suggested that the difference in beak shape between psittacosaurs and basal neoceratopsians could reflect differences in diet, with the narrow, pointed beak of basal neoceratopsians being used to penetrate harder plant material such as stems and large seeds. On the other hand, the relatively wider beak of psittacosaurs was suggested to have been more suitable for plucking large amounts of foliage, fruits and possibly small seeds in a single bite (Tanoue et al., 2009). This pattern is contrary to that hypothesised by Sereno et al., (2010), in which psittacosaurs are using the beak to crush nuts or hard seeds.

Further to this, angiosperm plants, which include most nut bearing flora and are considered the most nutritious plants, are shown to have only achieved taxonomic diversity in the Late Cretaceous despite an origin in the Early Cretaceous (Barrett and Willis, 2001). Psittacosaurs on the other hand, are known from the Early Cretaceous, when angiosperm plants are not as abundant as gymnosperms. It has been shown that gymnosperm plants would still have had enough energy rich material to support ceratopsian, and even sauropod diets (Hummel et al., 2008; Tanoue et al., 2009). Hence, it seems implausible that

psittacosaurs would seek out a non-abundant food source (nuts) when equally energetic and more abundant foodstuffs were available.

CONCLUSIONS

The research presented here shows the importance of accurately reconstructing soft tissues by using a case study of the basal ceratopsian dinosaur, *Psittacosaurus*. Previous reconstructions of the jaw adductor musculature of *Psittacosaurus gobiensis* included speculative avian-like features attaching to the jugal bar, modelled upon a superficial similarity between psittacosaurs and psittaciform birds (Sereno *et al.* 2010). The results of quantitative functional analysis and statistical assessments of these results have revealed the effects of the mPSM and mAMEV muscles during simulated feeding in *Psittacosaurus lujiatunensis*. The mPSM and mAMEV cause clear increases to the stress induced in the skull at all three tested bite positions, but also consequently increase the maximum producible bite force of this organism. Variation of the bite position is shown to have the greatest effect upon deformation of the finite element model. At the posterior-most tooth bite point, variation of the muscle load conditions and inclusion of the mPSM and mAMEV has a greater effect upon deformation of the finite element model than variation of the material properties of the skull. Despite the advantages of increased bite force, there is clear anatomical and evolutionary evidence against anteriorly situated enhancements to the jaw adductor musculature in psittacosaurs, and reconstructions of mPSM- or mAMEV-like muscles should be viewed with caution. ~~Ecological convergence between psittacosaurs and psittaciform birds cannot be founded upon the basis of superficial or etymological similarity alone.~~ A modelling approach such as the one employed here, allows us to test hypotheses of cranial function in psittacosaurs and make quantitative predictions on the palaeobiology of extinct taxa.

ACKNOWLEDGEMENTS

We thank Xu Xing (Institute of Vertebrate Paleontology and Paleoanthropology [IVPP], Beijing, China) for access to specimens in his care, Feng Yun (IVPP, Beijing, China) for CT scanning of the *Psittacosaurus lujiatunensis* specimen. This work was in part funded by grant BB/I011668/1 awarded to EJR.

LITERATURE CITED

Abdala F, Damiani R. 2004. Early development of the mammalian superficial masseter muscle in cynodonts. Palaeontologica Africana 40:23-29.

Abramoff MD, Magalhaes PJ, Ram SJ. 2004. Image Processing with ImageJ. Biophotonics International 11:36-42.

Barrett PM, Willis KJ. 2001. Did dinosaurs invent flowers? Dinosaur—angiosperm coevolution revisited. Biological Reviews 76:411-447.

Bryant HN, Russell AP. 1992. The role of phylogenetic analysis in the inference of unpreserved attributes of extinct taxa. Philosophical Transactions of the Royal Society of London B: Biological Sciences 337:405-418.

Button DJ, Rayfield EJ, Barrett PM. 2014. Cranial biomechanics underpins high sauropod diversity in resource-poor environments. Proceedings of the Royal Society of London B: Biological Sciences 281:20142114.

Carril J, Degrange FJ, Tambussi CP. 2015. Jaw myology and bite force of the monk parakeet (Aves, Psittaciformes). Journal of Anatomy 227:34-44.

Cox P, Fagan M, Rayfield E, Jeffery N. 2011. Finite element modelling of squirrel, guinea pig and rat skulls: using geometric morphometrics to assess sensitivity. Journal of Anatomy 219:696-709.

Creech J. 2004. Phylogenetic character analysis of crocodylian enamel microstructure and its relevance to biomechanical performance. Unpublished Masters thesis, Florida State University, Tallahassee.

Cuff AR, Rayfield EJ. 2015. Retrodeformation and muscular reconstruction of ornithomimosaurian dinosaur crania. PeerJ 3:e1093.

Fitton LC, Shi JF, Fagan MJ, O'Higgins P. 2012. Masticatory loadings and cranial deformation in *Macaca fascicularis*: a finite element analysis sensitivity study. Journal of Anatomy 221:55–68.

Galton PM. 1973. The cheeks of ornithischian dinosaurs. Lethaia 6:67-89.

Gordon A, Huxley A, Julian F. 1966a. Tension development in highly stretched vertebrate muscle fibres. The Journal of Physiology 184:143.

Gordon A, Huxley AF, Julian F. 1966b. The variation in isometric tension with sarcomere length in vertebrate muscle fibres. The Journal of ~~physiology~~ Physiology 184:170.

Haas G. 1955. The jaw musculature in *Protoceratops* and in other ceratopsians. American Museum Novitates 1729:1-24.

Hammer Ø, Harper DAT, Ryan PD. 2001. Past: Paleontological Statistics Software Package for Education and Data Analysis. Palaeontologia Electronica 4:1-9.

Hedrick BP, Dodson P. 2013. Lujiatun psittacosaurids: understanding individual and taphonomic variation using 3D geometric morphometrics. PloS ~~one~~ ONE 8:e69265.

Holliday CM. 2009. New insights into dinosaur jaw muscle anatomy. The Anatomical Record 292:1246-1265.

Holliday CM, Witmer LM. 2007. Archosaur adductor chamber evolution: integration of musculoskeletal and topological criteria in jaw muscle homology. Journal of Morphology 268:457-484.

Hummel J, Gee CT, Südekum K-H, Sander PM, Nogge G, Clauss M. 2008. In vitro digestibility of fern and gymnosperm foliage: implications for sauropod feeding ecology and diet selection. Proceedings of the Royal Society of London B: Biological Sciences 275:1015-1021.

Kemp TS. 2005. The origin and evolution of mammals. Oxford: Oxford University Press.

Knoll F. 2008. Buccal soft anatomy in *Lesothosaurus* (Dinosauria: Ornithischia). Neues Jahrbuch für Geologie und Paläontologie-Abhandlungen 248:355-364.

Lautenschlager S. 2013. Cranial myology and bite force performance of *Erlikosaurus andrewsi*: A novel approach for digital muscle reconstructions. Journal of ~~anatomy~~ Anatomy 222:260-272.

Lautenschlager S. 2015. Estimating cranial musculoskeletal constraints in theropod dinosaurs. Royal Society Open Science 2:150495.

Lautenschlager S, Witmer LM, Altangerel P, Rayfield EJ. 2013. Edentulism, beaks, and biomechanical innovations in the evolution of theropod dinosaurs. Proceedings of the National Academy of Sciences 110:20657-20662.

Lautenschlager S, Witmer LM, Altangerel P, Zanno LE, Rayfield EJ. 2014. Cranial anatomy of *Erlikosaurus andrewsi* (Dinosauria, Therizinosauria): new insights based on digital reconstruction. Journal of Vertebrate Paleontology 34:1263-1291.

Lautenschlager S, Brassey CA, Button DJ, Barrett PM. 2016. Decoupled form and function in disparate herbivorous dinosaur clades. Scientific reports 6:26495.

Lull RS, Wright NE. 1942. Hadrosaurian dinosaurs of North America. Geological Society of America Special Papers 40:1-272.

Metzger KA, Daniel WJ, Ross CF. 2005. Comparison of beam theory and finite-element analysis with in vivo bone strain data from the alligator cranium. The Anatomical Record Part A: Discoveries in Molecular, Cellular, and Evolutionary Biology 283:331-348.

Norman DB, Crompton AW, Butler RJ, Porro LB, Charig AJ. 2011. The Lower Jurassic ornithischian dinosaur *Heterodontosaurus tucki* Crompton & Charig, 1962: cranial anatomy, functional morphology, taxonomy, and relationships. Zoological Journal of the Linnean Society 163:182-276.

O'Higgins P, Cobb SN, Fitton LC, Gröning F, Phillips R, Liu J, Fagan MJ. 2011. Combining geometric morphometrics and functional simulation: an emerging toolkit for virtual functional analyses. Journal of Anatomy 218:3-15.

O'Higgins P, Milne N. 2013. Applying geometric morphometrics to compare changes in size and shape arising from finite elements analyses. Hystrix, the Italian Journal of Mammalogy 24:126-132.

Ostrom JH. 1964. A functional analysis of jaw mechanics in the dinosaur *Triceratops*.Postilla 88: 1-35.

Ostrom JH. 1966. Functional morphology and evolution of the ceratopsian dinosaurs. Evolution:290-308.

Parr WCH, Wroe S, Chamoli U, Richards HS, McCurry MR, Clausen PD, McHenry C. 2012. Toward integration of geometric morphometrics and computational biomechanics: New methods for 3D virtual reconstruction and quantitative analysis of Finite Element Models. Journal of Theoretical Biology 301:1-14.

Polly PD, Stayton CT, Dumont ER, Pierce SE, Rayfield EJ, Angielczyk KD. ~~In press~~2016. Combining geometric morphometrics and finite element analysis with evolutionary modeling: towards a synthesis. Journal of Vertebrate Paleontology 36:e1111225.

Sereno PC. 2012. Taxonomy, morphology, masticatory function and phylogeny of heterodontosaurid dinosaurs. ZooKeys 226:1-225.

Sereno PC, Xijin Z, Lin T. 2010. A new psittacosaur from Inner Mongolia and the parrot-like structure and function of the psittacosaur skull. Proceedings of the Royal Society of London B: Biological Sciences 277:199-209.

Tanoue K, Grandstaff BS, You HL, Dodson P. 2009. Jaw mechanics in basal Ceratopsia (Ornithischia, Dinosauria). The Anatomical Record 292:1352-1369.

Tokita M. 2003. The skull development of parrots with special reference to the emergence of a morphologically unique cranio-facial hinge. Zoological Science 20:749-758.

Tokita M, Kiyoshi T, Armstrong KN. 2007. Evolution of craniofacial novelty in parrots through developmental modularity and heterochrony. Evolution and Development 9:590-601.

Tokita M, Nakayama T, Schneider RA, Agata K. 2013. Molecular and cellular changes associated with the evolution of novel jaw muscles in parrots. Proceedings of the Royal Society of London B: Biological Sciences 280:20122319.

Walmsley CW, McCurry MR, Clausen PD, McHenry CR. 2013. Beware the black box: investigating the sensitivity of FEA simulations to modelling factors in comparative biomechanics. PeerJ 1:e204.

Witmer LM. 1997. The evolution of the antorbital cavity of archosaurs: a study in soft-tissue reconstruction in the fossil record with an analysis of the function of pneumaticity. Journal of Vertebrate Paleontology 17:1-76.

You H, Xu X. 2005. An adult specimen of *Hongshanosaurus houi* (Dinosauria: Psittacosauridae) from the Lower Cretaceous of Western Liaoning Province, China. Acta Geologica Sinica (English Edition) 79:168-173.

You H, Xu X, Wang X. 2003. A new genus of Psittacosauridae (Dinosauria: Ornithopoda) and the origin and early evolution of marginocephalian dinosaurs. Acta Geologica Sinica (English edition) 77:15-20.

Zapata U, Metzger K, Wang Q, Elsey RM, Ross CF, Dechow PC. 2010. Material properties of mandibular cortical bone in the American alligator, *Alligator mississippiensis*. Bone 46:860-867.

Zusi RL. 1993. Patterns of diversity in the avian skull. In: Hanken J, Hall BK, editors. The Skull, Volume 2: Patterns of Structural and Systematic Diversity. Chicago: University of Chicago Press. p 391-437.

FIGURE LEGENDS

Fig. 1. Cranial skeleton of *Psittacosaurus lujiatunensis* (IVPP V12617). (A) Physical specimen, (B) digital ~~representation~~ volume ~~redneringrendering~~ derived from CT scanning in left lateral view.~~.~~

Fig. 2. Digitally restored osteology of *Psittacosaurus lujiatunensis* in (A) left lateral, (B) dorsal and (C) frontal view. Individual elements of the cranium shown in different colors based on segmentation of CT data.

Fig. 3. Myological reconstruction of *Psittacosaurus lujiatunensis*. Origin and insertion sites and digitally reconstructed models in (A, B) lateral~~)~~, (C) frontal and (D) caudal view. (E) Coronal and (F) horizontal sections through the digital model. Bone in (B-D) rendered semi-transparent.

Fig. 4. Maximum bite force produced at each bite point for each of the four studied musculature arrangements. Range of bite force based on separate measurements obtained from the cranium and lower jaw FE models.

Fig. 5. Comparison of Von Mises stress distribution for different muscle arrangements and bite scenarios. Bite point simulated for (A-D) tip of the beak, (E-H) first tooth position, (I-L) last tooth position. Contour plots are scaled to 3 MPa peak stress for the cranium and 10 MPa for the mandible models.

Fig. 6. First two principal components from the geometric morphometric analysis of the (A) cranium and (B) mandible models subjected to different bite scenarios, muscle arrangements and material properties.

Jaw muscle	Volume [mm^3]	Force [N]
mAMP	25099	70.4
mAMEP	24682	60.1
mAMEM	17190	43.2
mAMES	37499	88.8
mPSTs	35330	66.5
mPTd	2229	11.6
mPTv	4650	20.1
mPSM	5620	29.9
mAMEV	7724	42.6

Table 1. Calculated muscle volumes and muscle forces for *Psittacosaurus lujiatunensis* based on digital reconstructions.

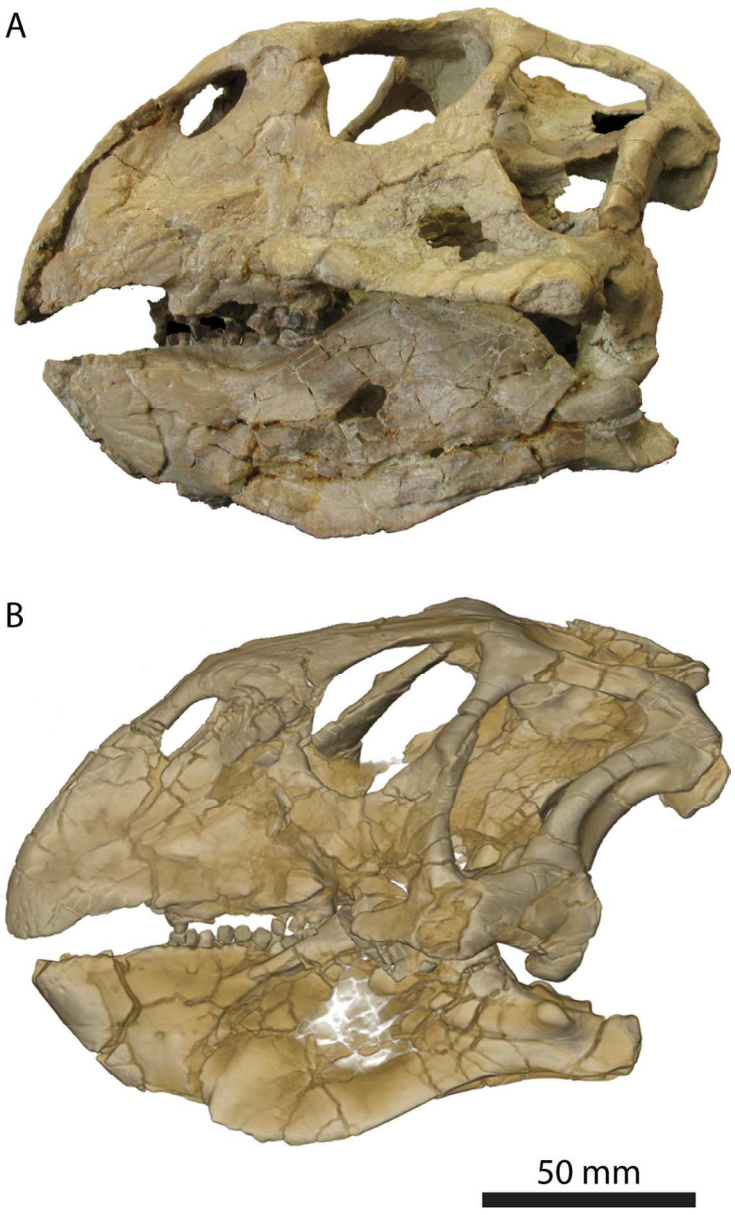

Fig. 1. Cranial skeleton of Psittacosaurus lujiatunensis (IVPP V12617). (A) Physical specimen, (B) digital volume rendering derived from CT scanning in left lateral view.

85x140mm (300 x 300 DPI)

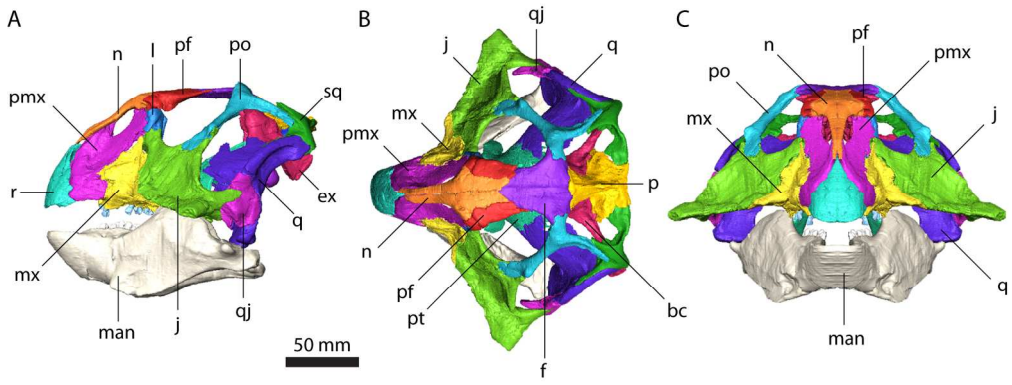

Fig. 2. Digitally restored osteology of Psittacosaurus lujiatunensis in (A) left lateral, (B) dorsal and (C) frontal view. Individual elements of the cranium shown in different colors based on segmentation of CT data.

177x67mm (300 x 300 DPI)

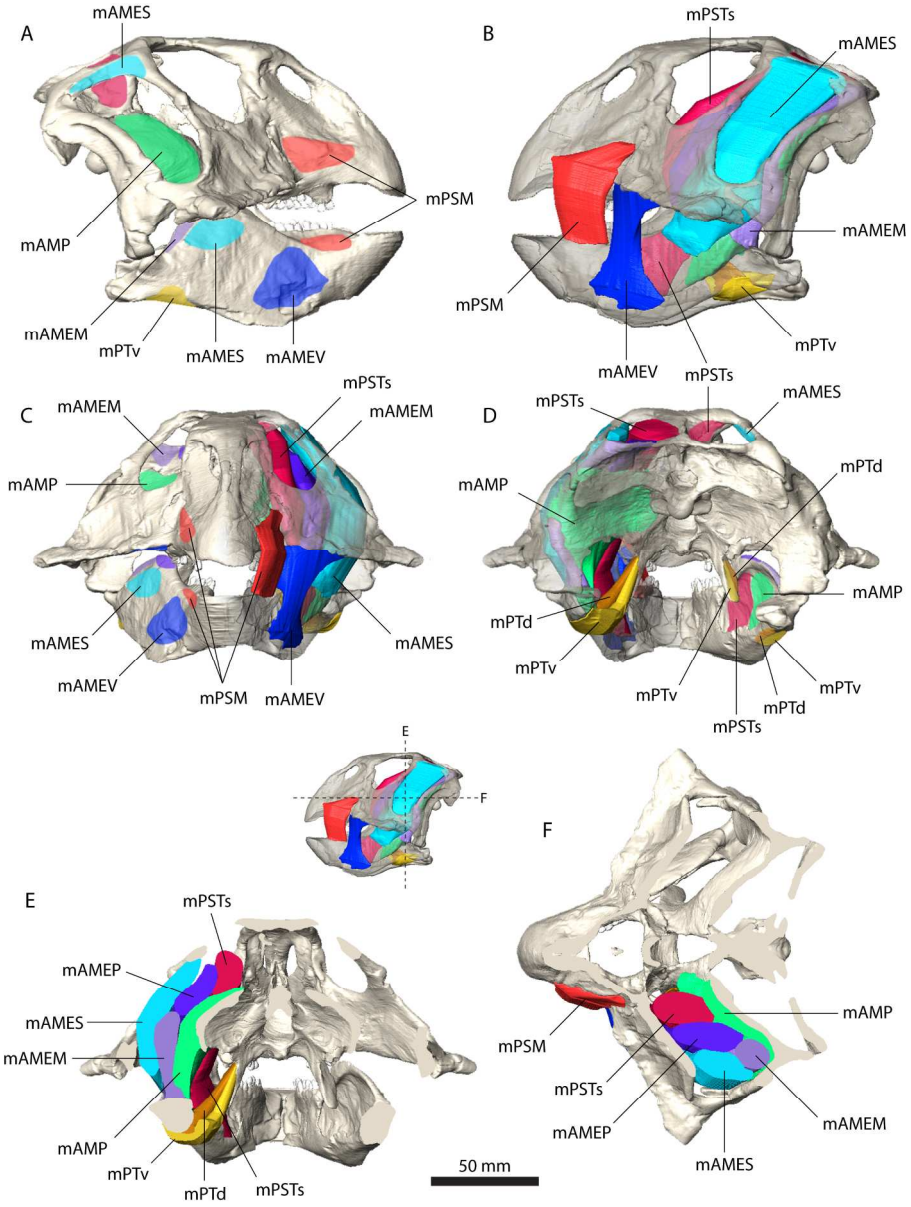

Fig. 3. Myological reconstruction of Psittacosaurus lujiatunensis. Origin and insertion sites and digitally reconstructed models in (A, B) lateral, (C) frontal and (D) caudal view. (E) Coronal and (F) horizontal sections through the digital model. Bone in (B-D) rendered semi-transparent.

176x234mm (300 x 300 DPI)

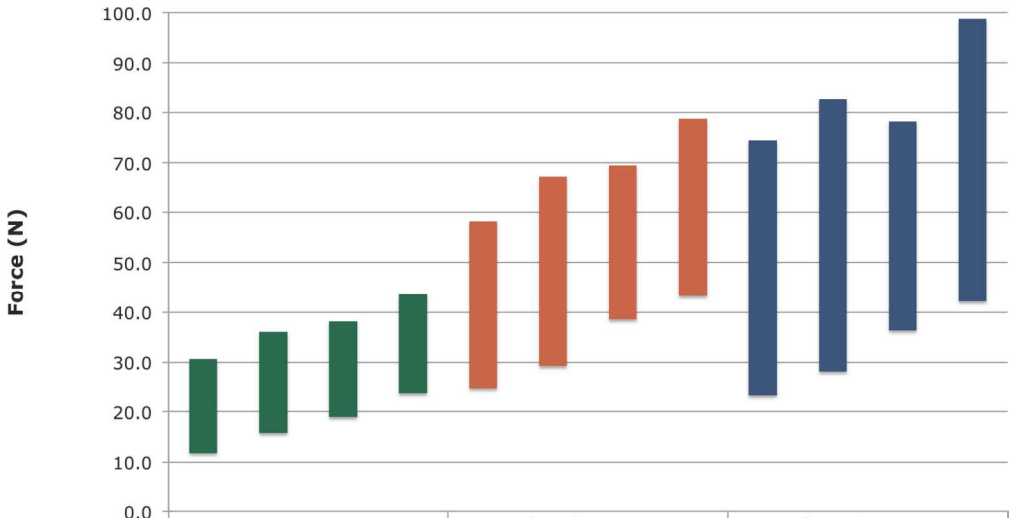

	Beak bite				Anterior-most tooth bite				Posterior-most tooth bite			
	Standard muscles	Standard + mPSM	Standard + mAMEV	Standard + mPSM + mAMEV	Standard Muscles	Standard + mPSM	Standard + mAMEV	Standard + mPSM + mAMEV	Standard Muscles	Standard + mPSM	Standard + mAMEV	Standard + mPSM + mAMEV
Measured on mandible	30.7	36.0	38.2	43.6	58.2	67.3	69.4	78.7	74.4	82.9	78.1	98.7
Measured on cranium	11.8	15.8	18.9	23.7	24.6	29.3	38.5	43.2	23.2	28.2	36.4	42.1

Fig. 4. Maximum bite force produced at each bite point for each of the four studied musculature arrangements. Range of bite force based on separate measurements obtained from the cranium and lower jaw FE models.

170x113mm (300 x 300 DPI)

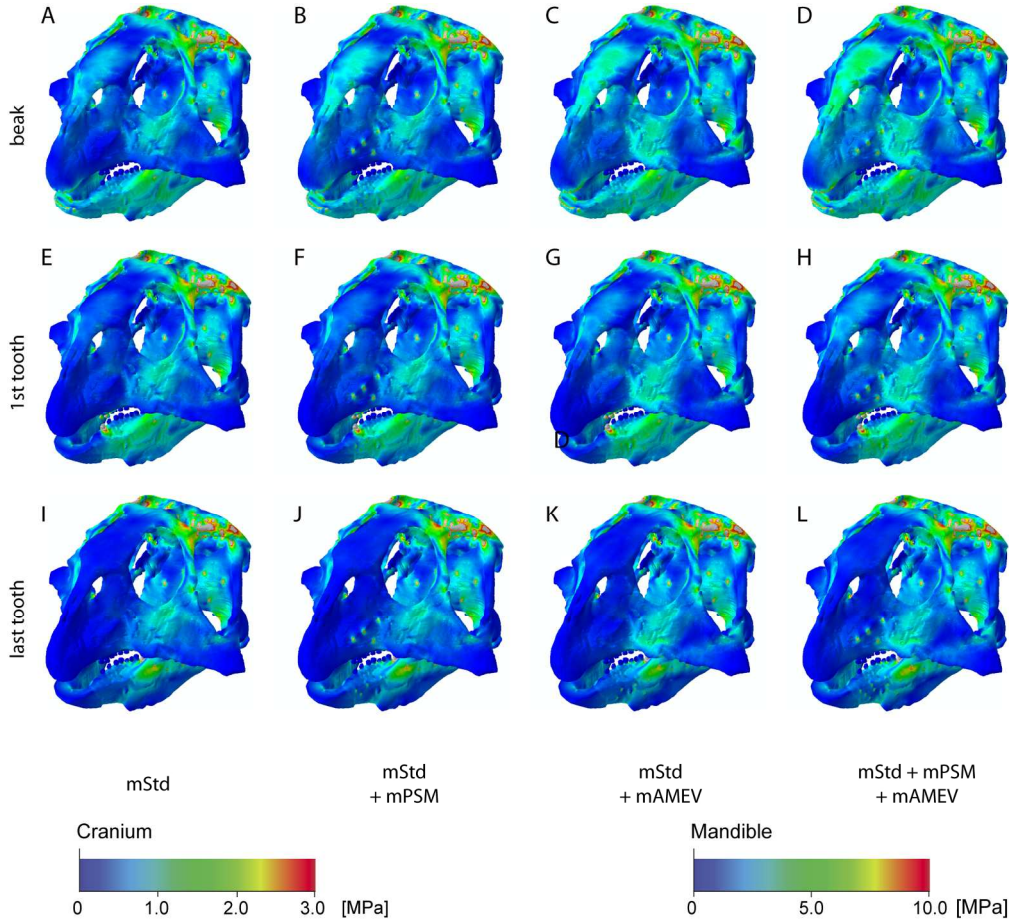

Fig. 5. Comparison of Von Mises stress distribution for different muscle arrangements and bite scenarios. Bite point simulated for (A-D) tip of the beak, (E-H) first tooth position, (I-L) last tooth position. Contour plots are scaled to 3 MPa peak stress for the cranium and 10 MPa for the mandible models.

176x161mm (300 x 300 DPI)

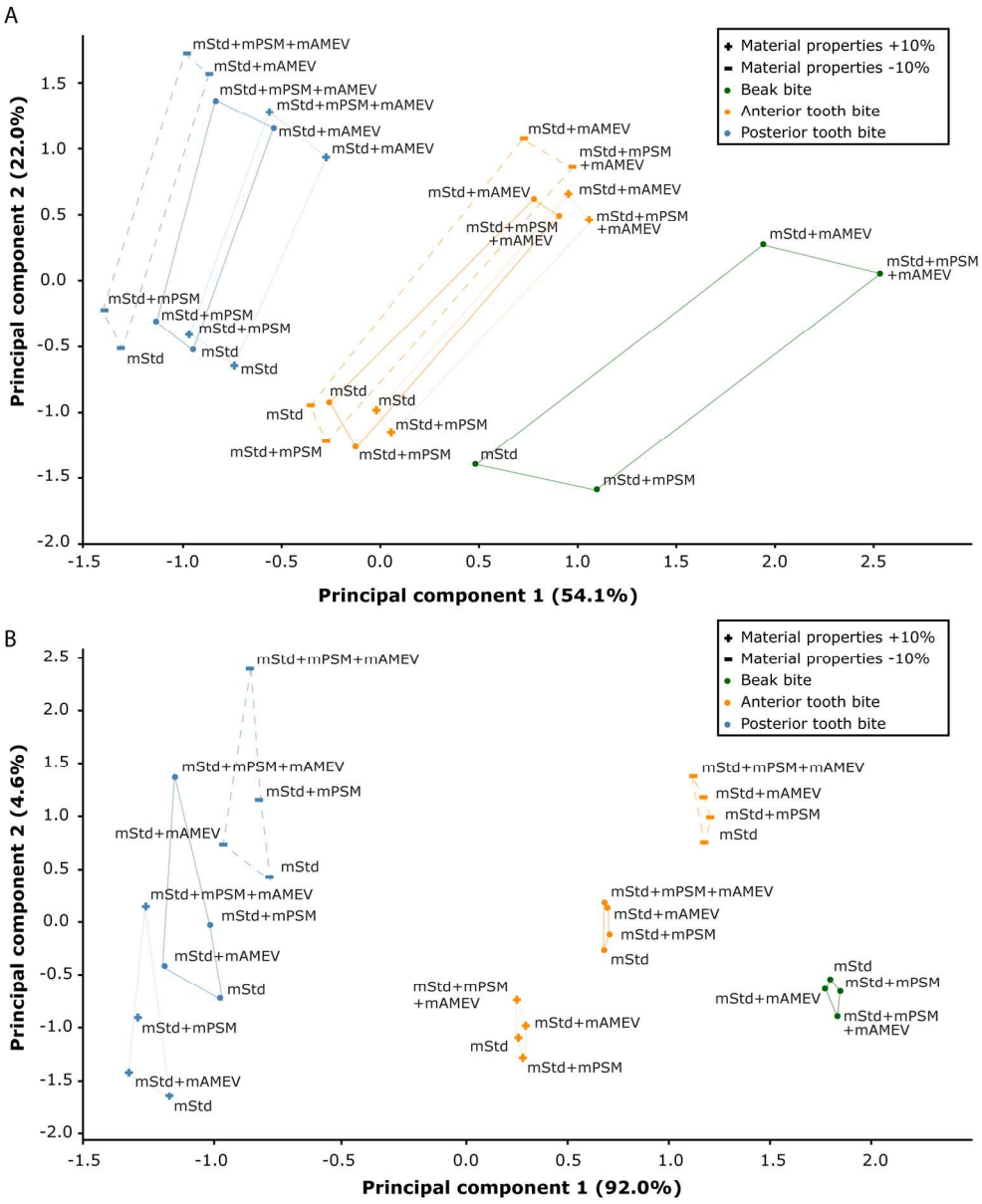

Fig. 6. First two principal components from the geometric morphometric analysis of the (A) cranium and (B) mandible models subjected to different bite scenarios, muscle arrangements and material properties.

174x213mm (300 x 300 DPI)